Inorganic Chemistry

Article

pubs.acs.org/IC

Multidimensional Open-Frameworks: Combinations of One-Dimensional Channels and Two-Dimensional Layers in Novel Bi/M Oxo-Chlorides

Minfeng Lü,[†,§] Almaz Aliev,[†] Jacob Olchowka,[†,‡] Marie Colmont,[†] Marielle Huvé,[†] Claudia Wickleder,[‡] and Olivier Mentré*[,†]

[†]Université Lille Nord de France, UMR 8181 CNRS, Unité de Catalyse et de Chimie du Solide (UCCS USTL), F-59655 Villeneuve d'Ascq, France

[‡]Inorganic Chemistry, Faculty for Science and Technology, University of Siegen, 57068 Siegen, Germany

[§]State Key Laboratory of Rare Earth Resource Utilization, Changchun Institute of Applied Chemistry, Chinese Academy of Sciences, Changchun 130022, P.R. China

Supporting Information

ABSTRACT: Here we discuss the synthesis and characterization of three novel bismuth oxo-chlorides ($[Bi_6Na_{0.5}O_{7.5}][Na_{0.5}Cl_3]_{channel}[Cl]_{layer}$; $[Bi_{17}PbO_{22}][Cl_6]_{channel}[Cl_3]_{layer}$; $[Bi_9(Pb_{0.2}Mn_{0.8})O_{12}][Cl_3]_{channel}[Cl_2]_{layer}$) which all show an original multidimensional crystal structure. It is formed of two-dimensional (2D)-layered blocks separated by Cl^- layers. The blocks are porous with triangular one-dimensional (1D)-Cl^- channels with various section sizes. This multidimensional feature is unique in the field of Bi and Pb oxo-halides, while so far only 1D or 2D halides units have been reported. The stability of the framework is allowed by Bi^{3+}/M^{n+} aliovalent substitution to balance charge neutrality. The channel and tunnel walls are formed by edge-sharing $O(Bi,M)_4$ oxocentered tetrahedra, while the triangular tunnel junctions are achieved by $O(Bi,M)_5$ pyramids. The three compounds are rather stable, but only $[Bi_6Na_{0.5}O_{7.5}][Na_{0.5}Cl_3]_{tunnel}[Cl]_{layer}$ was obtain as a single-phase material so that its photoluminecence properties have been investigated. It shows an unusual red bright luminescence with a maximum at 14150 cm^{-1} at low temperatures due to Bi^{3+} transitions that are well explained by the Bi-Cl bonding scheme.

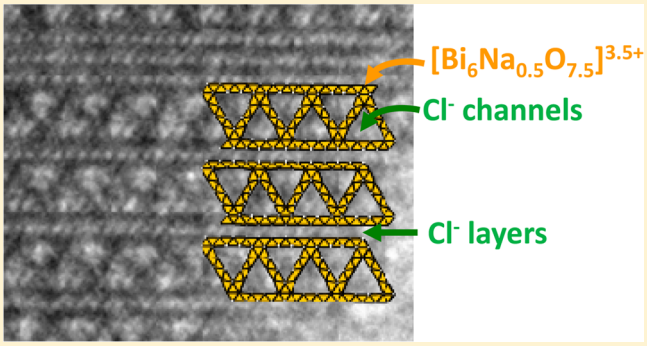

INTRODUCTION

Low-dimensional solid-state materials often exhibit unusual anisotropic physical and chemical properties. In this context, the search for layered bismuth oxo-halides has been recently intensified owing to luminescence,[1] selective oxidation catalysts,[2,3] and multiferroic properties.[4] Most often, these compounds are based on layered intergrowths of bismuth oxide blocks, separated by halide layers. The most famous and simplest phases are known as the Sillén series,[5,6] that is, $MBiO_2Cl$ (X_1) (M^{2+} = Cd, Ca, Pb, etc.),[7−9] BiOCl (X_2),[10] and $Ca_{1.25}Bi_{1.5}O_2Cl_3$ (X_3),[11,12] consisting of α-PbO (or fluorite) $[M_2O_2]^{2+}$ layers intergrown with single [X_1], double [X_2], or triple $[M'_xX_3]$ halide layers. For instance, in the X_3-type $Ca_{1.25}Bi_{1.5}O_2Cl_3$ the interstitial calcium atom is 75% occupied leading to deficient $[Ca_{0.75}Cl_3]$ layers. The intergrowths between verstatile oxide and halide subunits in varying sequences lead to new structures of increasing complexity,[13,14] and additionally several [X_n] thicknesses could coexist in the same compound such as in $SrBi_3O_4Cl_3(X_1X_2)$,[15] $Bi_{1.73}Ca_{2.74}Cl_4O_{3.32}$ (X_1X_3),[16] and $Ca_{0.80}Bi_{3.80}O_4Cl_5(X_2X_3)$.[17] A selection of important crystal structures is shown in the Supporting Information. However, the richness of the crystal chemistry of relevant oxide blocks is governed not only by the asymmetric coordination of Bi^{3+} cations due to their stereoactive $6s^2$ lone pair [13] but also by their ability to form oxocentered OBi_n polyhedra stacked into zero-dimensional (0D), one-dimensional (1D), two-dimensional (2D), and three-dimensional (3D) frameworks.[18] The typical Bi^{3+}-O bond valence being 0.596 valence units (v.u.) (slightly higher than the 0.5 v.u. needed to form ideal OBi_4 tetrahedra [19]), it most often results in distorted OBi_4 tetrahedra that can admit the copresence of other M^{n+} cations into $O(Bi,M)_4$ units, for relaxing the oxygen bonding scheme. The great diversity of aliovalent M^{n+} cations that can be incorporated into the $O(Bi,M)_4$ tetrahedral bricks makes this class of inorganic compounds a gold mine of inspiration for the discovery of novel structural motifs with unexpected properties. This alternative "oxocentered" description was recently reviewed for all possible AM_4 anion-centered tetrahedra in ref 18. As an

Received: October 11, 2013
Published: December 12, 2013

Table 1. Conditions and Results of the Attempts to Reproduce the Compounds in the Form of Powder[a]

n	formulation	*T*, K	conditions	phase found
1	$Bi_6NaO_{7.5}Cl_4$	873	non-evacuated tube	pure, $Bi_6NaO_{7.5}Cl_4$
		873	air	$Bi_6NaO_{7.5}Cl_4$; $NaBi_3O_4Cl_2$
		923	air	$NaBi_3O_4Cl_2$
		873	evacuated tube	$Bi_6NaO_{7.5}Cl_4$,; Bi_2O_3
2	$Bi_{17}PbO_{22}Cl_9$	973	non-evacuated tube	major, $Bi_{17}PbO_{22}Cl_9$; minor, s.d.; minor,$Pb_3O_2Cl_2$, minor, $Pb[ClO_2]_2$
		973	air	u.p
		1023	non-evacuated tube	major, $Bi_{17}PbO_{22}Cl_9$; minor, s.d.; minor, $Pb_3O_2Cl_2$; minor, $Pb[ClO_2]_2$
3	$Bi_9O_9Cl_4(Pb_{0.2}Mn_{0.8})O_3Cl$	873	non-evacuated tube	major, $Bi_9O_9Cl_4(Pb_{0.2}Mn_{0.8})O_3Cl$; minor, s.d.
		873	evacuated tube	u.p; BiOCl
		923	air	u.p
		923	non-evacuated tube	u.p

[a]s.d. refers to slight chemical deviation from formulation, and u.p. denotes many unknown phases.

Table 2. Crystal Data, Measurement, and Structural Refinement Parameters of $Bi_6NaO_{7.5}Cl_4$, $Bi_{17}PbO_{22}Cl_9$ and $Bi_9(Pb_{0.2}Mn_{0.8})O_{12}Cl_5$.

	$Bi_6NaO_{7.5}Cl_4$	$Bi_{17}PbO_{22}Cl_9$	$Bi_9(Pb_{0.2}Mn_{0.8})O_{12}Cl_5$
	Crystal Data		
crystal symmetry	orthorhombic *Cmcm*	monoclinic(twinned) *C*2/*m*	orthorhombic *Cmcm*
symmetry space group			
a (Å)	3.85170(10)	38.9122(18)	3.8695(2)
b (Å)	45.4530(9)	3.8850(2)	31.7369(15)
c (Å)	15.5814(3)	11.6784(6)	15.7602(7)
β (deg)		95.729(3)	
V (Å^3)	2727.86(10)	1756.65(15)	1935.45(16)
Z	8	2	4
Dx (g/cm^3)	7.4907	8.3742	8.001
μ (mm^{-1}) (for $\lambda_{K\alpha}$ = 0.7107 Å)	83.251	96.128	84.31
appearance	transparent needle	pale green needle	transparent needle
	Data Collection		
λ(Mo Kα) (Å)	0.71073	0.71073	0.71073
scan mode	ω and φ	ω and φ	ω and φ
$\theta_{(min-max)}$ (deg)	1.58−33.1	1.75−33.11	1.3−28.2
R(int) (%)	3.49	4.6	0.036
recording reciprocal space	$-5 \le h \le 5$	$-58 \le h \le 50$	$-4 \le h \le 5$
	$-67 \le k \le 68$	$-5 \le k \le 5$	$-25 \le k \le 24$
	$-23 \le l \le 23$	$-17 \le l \le 17$	$-18 \le l \le 18$
	Refinement		
measured, independent, collected refl.	2988, 2484, 19816	2893, 2312, 13533	23978, 2401, 1726
no. of refined parameters	125	136	72
refin. method,	F	F	F
R1(F^2)(obs)/R1(F^2)(all)	0.0215/0.033	0.0568/0.0720	0.047
wR2(F^2)(obs)/wR2(F^2)(all)	0.0258/0.0263	0.0722/0.0739	0.067
$\Delta\rho_{max}/\Delta\rho_{min}$ (e Å^{-3})	2.72/−2.98	11.85/−9.97	4.77/−4.76
twin ratio		0.276(6)	

illustration, in the case of bismuth oxo-halides, the easy substitution of OBi_4 by $O(Bi,Pb)_4$ enabled the recent design of the $[Pb_nBi_{10-n}O_{13}][Bi_2O_2]_nCl_{4+n}$ series [20] related to the parent $Bi_{24}O_{31}Cl_{10}$ Arppe's compound.[21] In these series single (X_1) layers isolate Bi/Pb/O crenel-layers with various step-size, *n* = 1, 2, 3, 4 $O(Bi,Pb)_4$ tetrahedra. More rarely, Cl^- anions can occupy 1D channels in porous Bi based frameworks, such as found in $Bi_{12}O_{15}Cl_6$.[22] The potentiality to combine in the same compound 2D-layers and 1D channels of halides had not been explored yet but was successfully achieved in this work. We used the incorporation of alien cations (M = Na^+, Pb^{2+}, Mn^{2+}) as partially substituent of Bi^{3+}, leading to three original multidimensional crystal structures in the chloride rich part of the Bi_2O_3-BiOCl phase diagram. Luminescence properties have been tested since some Sillén bismuth oxyhalide phases are reported to show a blue luminescence under UV excitation at room temperature.[23]

(1). EXPERIMENTAL SECTION

$Bi_6NaO_{7.5}Cl_4$ (I). Single crystals of compound (I) have been obtained from the slow cooling of a mixture of Bi_2O_3/BiOCl/Na_2O_2/Co_3O_4 in the molar ratio 18:36:3:4. Since the starting reagent Na_2O_2 is air sensitive, manipulations were carried out under an inert gas atmosphere (glovebox). The mixtures were then put into alumina crucibles with lids and vacuum sealed in quartz tubes. Heat treatments

dx.doi.org/10.1021/ic402578m | Inorg. Chem. 2014, 53, 528−536

Table 3. BVS of $Bi_6NaO_{7.5}Cl_4$, $Bi_{17}PbO_{22}Cl_9$ and $Bi_9(Pb_{0.2}Mn_{0.8})O_{12}Cl_5$

$Bi_6NaO_{7.5}Cl_4$			$Bi_{17}PbO_{22}Cl_9$			$Bi_9(Pb_{0.2}Mn_{0.8})O_{12}Cl_5$			
atom	v_{Bi}[a]	V_{Na}[a]	atom	v_{Bi}[a]	v_{Pb}[a]	atom	v_{Bi}[a]	V_{Mn}[a]	V_{Pb}[a]
Bi1	3.26		Bi1	3.36		Bi1	3.11		
Bi2	3.19		Bi2	2.98		Bi2	3.38		
Bi3	3.20		Bi3	2.92		Bi3	2.83		
Bi4	2.75		Bi4	2.88		Bi4	3.25		
Bi/Na5	3.18	1.28	Bi5	3.24		Bi5	2.87		
Bi6a	2.93		Bi6	3.26		Mn/Pb6		2.00	2.74
Bi6a	2.63		Bi/Pb7	2.57	2.60				
Bi/Na7	3.03	1.22	Bi/Pb8	2.46	2.52				
Bi/Na8 Na9	2.90	1.17 0.77	Bi9	2.56					

[a] (R, b) parameters being for Pb^{2+}-O (1.963, 0.49),[28] Pb^{2+}-Cl (2.53, 0.37), Bi^{3+}-O (2.094, 0.37), Bi^{3+}-Cl (2.48, 0.37), Na^{+}-O (1.756, 0.37), Na^{+}-Cl (2.15, 0.37), Mn^{2+}-O (1.79, 0.37), Mn^{2+}-Cl (2.13, 0.37).

were performed at 1173 K for 12 h and slowly cooled down to 973 K for 50 h before switching off the furnace. EDX analyses of isolated transparent needle-like crystals exclude the presence of cobalt as a constituent element but shows the copresence of Bi/Na/Cl with ratio 6:1.2:5 using a semiquantitative analysis (Supporting Information, Figure S1).

The $Bi_6NaO_{7.5}Cl_4$ polycrystalline sample was prepared afterward by solid state reaction. Bi_2O_3 (Aldrich, 99.9%), BiOCl (Prolabo, ultrapure), and Na_2CO_3 (Aldrich, 99.5%) were used as starting materials in stoichiometric amounts. The reagents were weighed, placed in an agate mortar, closely grinded and homogenized, deposited in a closed gold tube, and then sealed into a quartz tube in air. The treatment was performed at 873 K for 24 h before quenching. It was obtained as a single phase, see Table 1. The lattice parameters refined from the powder diffraction pattern lead to a C-centered orthorhombic with parameters a = 3.8519(5) Å, b = 45.4738(46) Å, and c = 15.5938(17) Å in good agreement with results from the single crystal data (see Table 2).

$Bi_{17}PbO_{22}Cl_9$ (II). The transparent needle-shaped crystals of compound (II) were found in the melt of the mixture Bi_2O_3/BiOCl/PbO_2/MnO_2 (molar ratio = 3:6:1:1). It was also placed into a gold tube, closed tightly, and then vacuum sealed in a silica tube. Heat treatments were performed at 1253 K for 2.5 h then quickly dropped to 1023 K, and finally slowly cooled down to 923 K during 100 h. EDX analyses indicate the presence of Bi, Cl, and Pb as constituent element with [Bi+Pb]/Cl ratio of 18:11. The Bi/Pb ratio is hardly estimable since the co-presence of both cations is revealed by a shoulder at the M_α-peak (Supporting Information, Figure S2).

Several methods have been used to prepare single-phase polycrystalline (II) (see a selection in the Table 1). The most relevant result was obtained from the stoichiometric mixture of Bi_2O_3 (Aldrich, 99.9%), BiOCl (Prolabo, ultrapure) and PbO (Aldrich, 99.9%) heated at 973 K for 24 h in a non-evacuated quartz ampule leading to compound (II) as a major component with additional minor phases. The monoclinic cell parameters refined from the powder diffraction are a = 38.8140(26) Å, b = 3.8806(2) Å, c = 11.6400(13) Å, β = 95.599(8)°.

$Bi_9(Pb_{0.2}Mn_{0.8})O_{12}Cl_5$ (III). Single crystals were found in a polyphasic melt obtained as follows: the BiOCl/Bi_2O_3/PbO/MnO_2 mixture (ratio 3:3:1:3) was ground, loaded into a gold tube closed tightly, and placed into a quartz tube and sealed under vacuum, then heated slowly up to 1173 K at a rate 50 K/h, then left during 10 h and cooled down to 873 K at a rate 3 K/h, then the furnace was switched off. The ratio of the elements Bi/Pb/Mn/Cl determined using a microprobe analysis are 8.2/0.4/0.8/5.0 in good agreement with the refined stoechiometry.

Among several attempts, the corresponding powder was obtained as a main polycrystalline phase from the stoichiometric mixture of BiOCl, Bi_2O_3, and MnO heated at 873 K deposited in a sealed gold tube, itself sealed in a non-evacuated quartz tube, after intermediate grinding, see Table 1. The lattice parameters refined from the powder diffraction are a = 3.8661(2) Å, b = 31.7152(18) Å, c = 15.7381 (10) Å.

Single Crystal XRD. Data for all the investigated samples have been collected using a Bruker Apex Duo diffractometer with a Mo-IμS microfocus tube (λ = 0.71073 Å). The intensity data have been extracted from the collected frames using the program SAINT-Plus 6.02.[24] The lattice parameters have been defined from the complete data set. Absorption corrections have been performed using multiscan methods using SADABS.[25] The data collection and pertinent data of the refinements for all single crystals studied in this work are gathered in the Table 2.

X-ray Powder Diffraction. The analysis of all powder samples have been performed at room temperature in the angular 2Θ range of 5−80° with the scan step width of 0.02° using the D8 Advance Bruker AXS diffractometer.

Elemental Analysis. For compounds (I) and (II) EDX analysis (Supporting Information, Table S1) was performed on a Scanning Electron Microscope (SEM) working on a HITACHI S4700 microscope at 20 kV acceleration voltage and a current of 15 μA at different magnifications. The ratios were determined using a semiquantitative routine deconvolution. For compound (III) the quantitative analysis was conducted on EPMA Cameca SX100 microprobe operated at 15kV, with the current of the beam being 15 nA.

Photoluminescence. Excitation and emission spectra were collected on a FluoroMax HORIBA fluorescence spectrometer within the spectral range of 250−850 nm using excitation and emission slit widths of 1 nm. A liquid Helium closed-cycle cryostat was used to perform measurements at 10 K and temperature-dependent measurements. The emission spectra were corrected for the photomultiplier sensitivity, and the excitation spectra were corrected for the lamp intensity. For decay time measurements, the same equipment with a Xenon flash lamp as an excitation source was used.

Transmission electron microscopy (TEM) studies were performed on a Philips CM30. The polycrystalline materials (prepared as detailed above) were crushed and dropped in the form of aqueous or alcohol suspensions on carbon-supported copper grids followed by evaporation under ambient conditions. In these conditions of preparation the crystals are mainly oriented preferentially perpendicular to the channel directions. For the three tested samples, a number of different crystals were examined to reach the pertinent projection. The computer simulated HREM images were calculated using the JEMS program.[26]

(2). RESULT AND DISCUSSION

$Bi_6NaO_{7.5}Cl_4$ (I). The crystal structure of compound (I) was solved in the space group *Cmcm* (parameters a = 3.8517(1) Å, b = 45.4530(9) Å, and c = 15.5814(3) Å). The lattice parameters $a \sim 3.9$ Å and $c \sim 4 \times 3.9$ Å suggest a layered structure along the b-axis, built from the stacking of $[Bi_2O_2]^{2+}$ fluorite layers, (i.e., 3.9 Å corresponds to $\sqrt{2}/2a_{fluorite}$), compatible with Sillén phases derivatives.[5−12,27] Bismuth and chlorine atoms were found from direct methods using Shelxs.[28]

dx.doi.org/10.1021/ic402578m | Inorg. Chem. 2014, 53, 528−536

Table 4. Bond Lengths (Å) of $Bi_6NaO_{7.5}Cl_4$

atom1	atom2	*d*	atom1	atom2	*d*
Bi1	2×Cl1	3.1462(8)	Bi6a	2×Cl2	3.164(6)
	2×Cl3	3.1979(17)		O4	2.848(7)
	O1	2.191(5)		2×O5	2.282(4)
	2×O3	2.252(3)		O7	2.260(9)
	O3	2.303(5)		O8	2.371(9)
Bi2	2×Cl2	3.1408(16)		2×O9	2.744(10)
	2×Cl3	3.3619(18)		2×O9	3.112(10)
	2×O1	2.240(3)	Bi6b	2×Cl2	3.191(6)
	O3	2.413(5)		O4	2.479(13)
	O4	2.129(6)		2×O5	2.498(8)
Bi3	2×Cl5	3.3135(18)		O7	2.257(11)
	2×Cl5	3.4107(18)		O8	2.770(10)
	O5	2.180(5)		2×O9	2.454(9)
	O6	2.260(5)		2×O9	2.860(10)
	2×O8	2.226(3)	Bi/Na7	4×Cl5	3.3298(18)
Bi4	2×Cl1	3.421(2)		2×O5	2.261(5)
	4×O4	2.447(3)		2×O7	2.238(4)
	2×O9	2.179(10)	Bi/Na8	4×Cl5	3.2985(18)
Bi/Na5	2×Cl2	3.1619(16)		2×O2	2.255(4)
	2×Cl4	3.1672(15)		2×O6	2.291(5)
	O2	2.248(4)	Na9	4×Cl3	2.880(3)
	2×O6	2.265(3)		2×Cl4	2.966(5)
	O8	2.260(5)			

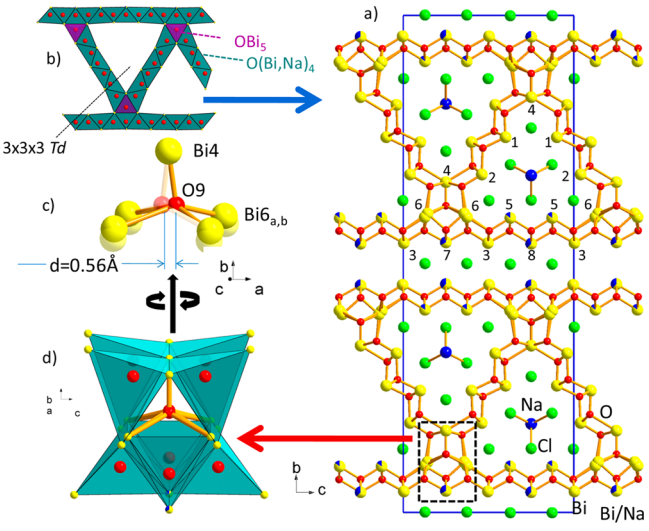

Figure 1. (a) Projection of the structure of $Bi_6NaO_{7.5}Cl_4$ along the *a* axis with Bi and Bi/Na labels. (b) The size of the channel: the channel walls are formed by oxocentered $O(Bi,Na)_4$ tetrahedra (dark green), while the connection of $O(Bi,Na)_5$ square-pyramid is highlighted in purple. (c) Geometry of the OM_5 square pyramid coordination along [101] axis. (d) Local structure of the tunnel junction.

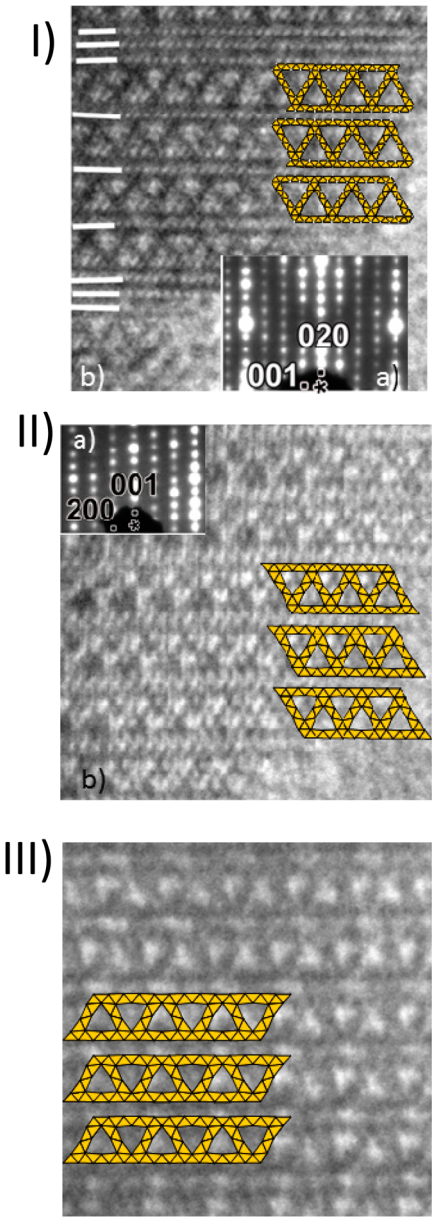

Figure 2. TEM images for (I) Compound I: (a) [100] electron diffraction zone axis (EDZA) pattern, (b) corresponding TEM image with the projected structure along the *a* axis. The white lines indicate the position of the Cl^- layers between the $[Bi_6Na_{0.5}O_{7.5}]^{3.5+}$ blocks. (II) Compound II: (a) [010] EDZA pattern, (b) corresponding TEM image with projected tunnel structure. (III) compound III: [100] TEM image and structure.

Oxygen atoms were further located from Fourier-difference maps. As commonly found in such compounds,[20] several clues (residual electron density peaks, large thermal parameters, ...) suggest a certain degree of disorder within the refined topology. Mixed Bi/Na occupancy was assumed for Bi/Na(5) (85%−15%), Bi/Na(7) (67%−33%), and Bi/Na(8) (62%−38%) because of overly large values of thermal parameters. The occupancies were refined under restrictions for the conservation of the electric neutrality, leading to acceptable thermal parameters. Finally the split of Bi(6) into two satellites $Bi(6)_{a-b}$ improves the convergence by more than 2% on *R* values. A similar feature is rather common in Birich phases such as Bi_2O_3 derivatives.[29] Also the atom O(9) is shifted 0.28 Å out of the mirror plane leading to a 50% occupied position, and in probable connection with the disorder on the Bi(6) site. The final *R1 factor is* 2.15% for all 2988 reflections and 3.03% for 2484 observed reflections ($I > 2\sigma(I)$). The refined positional and thermal parameters are given in Supporting Information, Tables S2, S3. Pertinent distances are listed in the Table 4.

A projection of the structure of (I) is shown in Figure 1a. It may be described as a layered structure between complex $[Bi_6Na_{0.5}O_{7.5}]^{3.5+}$ blocks, isolated by single Cl^- layers perpendicular to *b*. The blocks contain tunnels filled by Cl^- ions and Na^+ ions at their middle, Figure 1b. The [100] TEM

dx.doi.org/10.1021/ic402578m | *Inorg. Chem.* 2014, 53, 528−536

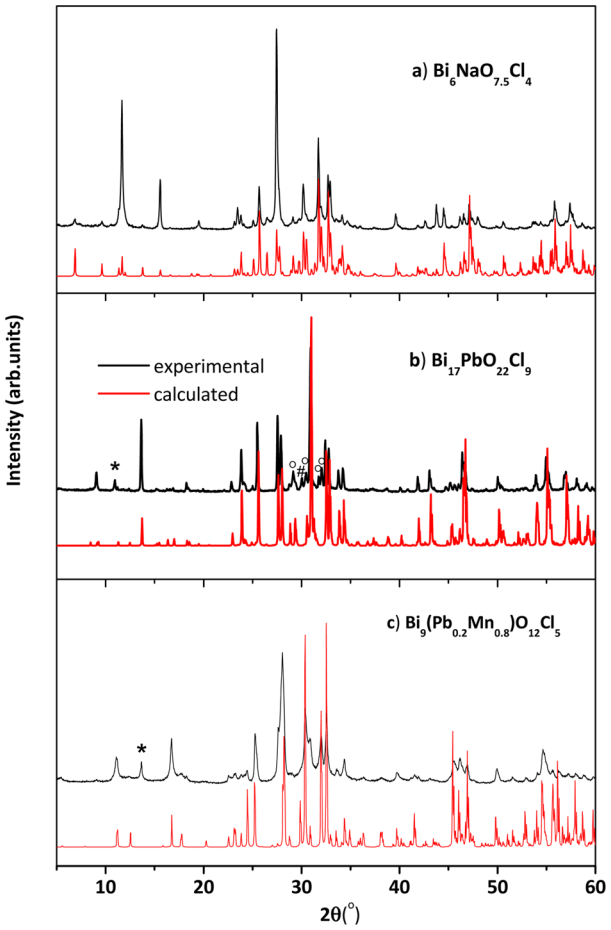

Figure 3. X-ray powder patterns for (a) $Bi_6NaO_{7.5}Cl_4$, (b) $Bi_{17}PbO_{22}Cl_9$, and (c) $Bi_9O_9Cl_4(Pb_{0.2}Mn_{0.8})O_3Cl$ of the experimental (black) and calculation from the single crystal XRD data (red). The markers refer to (*) phase with a slight chemical deviation; (#) $Pb_3O_2Cl_2$, and (○) $Pb[ClO_2]_2$ impurities.

image (Figure.2.I) reproduces perfectly the arrangement between the triangular tunnels. The superimposition of the structure is positioned with the help of a simulation for a defocalization of 40 Å and a thickness of 70 Å. One can notice as intergrowth defects the presence of double or triple Cl^- layers (white lines on the Figure 2.I), which indicates the possibility of intergrowth with the BiOCl crystal structure. Taking into account the refined crystal structure in absence of faults, the strict segregation of chlorides into the 1D and 2D subunits leads to the formula $[Bi_6Na_{0.5}O_{7.5}]$-$[Na_{0.5}Cl_3]_{channel}[Cl]_{layer}$. As discussed above, it is often more convenient to describe such crystal structure in terms of oxo-centered polyhedra. Here the channel walls contain $[Bi_{2-x}Na_xO_2]_{4n}^{(2-2x)+}$ layers parallel to the (a,c) plane and formed of edge-sharing $O(Bi,Na)_4$ tetrahedra. The atom $O(9)Bi_5$ square-pyramid joins the layers with two 120°-tilted finite ribbons (three OBi_4 wide) leading to triangular channels, Figure 1c–d. In detail, every O(1)-O(8) oxygen atoms form oxo-centered tetrahedra with 2.13 Å < O-Bi < 2.84 Å, while the $O(9)Bi_5$ square-pyramid is distorted because of O(9) off-centering. It leads to one short O(9)-Bi(4) bond of 2.18(2) Å, two medium O(9)-Bi(6) bonds of 2.45(1)–2.74(1) Å, and two long O(9)-Bi(6) bonds of 2.86(1)–3.11(1) Å.

If one focuses on the coordination of the cations, it is remarkable that all Bi(1) to Bi/Na(8) sites are coordinated in

Table 5. Bond Lengths (Å) of $Bi_{17}PbO_{22}Cl_9$

atom1	atom2	*d*	atom1	atom2	*d*
Bi1	2×Cl3	3.111(6)	Bi6	2×Cl3	3.225(5)
	2×Cl4	3.094(7)		2×Cl5	3.222(6)
	2×O1	2.277(8)		2×O6	2.226(9)
	O4	2.22(2)		O6	2.21(2)
	O7	2.22(2)		O10	2.28(2)
Bi2	2×Cl1	3.402(6)	Bi/Pb7	2×Cl3	3.158(7)
	2×Cl1	3.279(5)		O4	2.67(2)
	O1	2.31(2)		O5	2.26(2)
	O3	2.21(2)		2×O8	2.447(10)
	2×O7	2.252(9)		O10	2.60(3)
Bi3	2×Cl1	3.390(5)		2×O11	2.70(3)
	2×Cl2	3.3057(10)	Bi/Pb8	2×Cl4	3.161(7)
	O1	2.34(2)		2×O3	2.453(11)
	2×O4	2.265(8)		O5	2.30(2)
	O8	2.21(2)		O7	2.70(2)
Bi4	2×Cl1	3.322(6)		O9	2.60(3)
	2×Cl2	3.3552(10)		2×O11	2.71(4)
	O3	2.27(2)	Bi9	2×Cl5	3.329(5)
	2×O5	2.273(9)		O2	2.813(18)
	O8	2.28(2)		O6	2.83(2)
Bi5	2×Cl4	3.230(5)		2×O9	2.447(14)
	2×Cl5	3.233(6)		2×O10	2.457(12)
	O2	2.223(19)		O11	2.32(4)
	2×O2	2.232(10)			
	O9	2.27(2)			

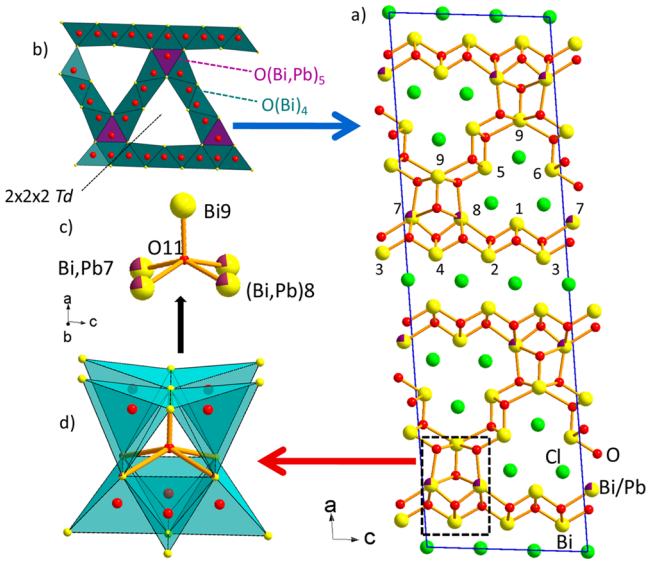

Figure 4. (a) Projection of the structure of $Bi_{17}PbO_{22}Cl_9$ along the *b* axis. (b)The size of the channel: the channel walls are formed by oxocentered OBi_4 tetrahedra (dark green), while the connection of $O(Bi,Pb)_5$ square-pyramid is highlighted in purple. (c) Geometry of the OM_5 square pyramid coordination. (d) Local structure of the tunnel junction.

typical tetragonal antiprisms. In detail, Bi(1), Bi(2), Bi(3), Bi/Na(5), Bi/Na(7), and Bi/Na(8) are surrounded by four Cl and four O atoms, while Bi(4) and $Bi(6)_{a/b}$ by two Cl and six O atoms. Finally, the *in-plane* section of the triangular channels has 3 × 3 × 3 tetrahedra and appears original as further discussed. At their centers, Na(1) is coordinated by four Cl(3) (2.88 Å) and two Cl(4) (2.97 Å) which form of a deformed trigonal-prism. The Na-Cl distances do not differ very much

dx.doi.org/10.1021/ic402578m | Inorg. Chem. 2014, 53, 528–536

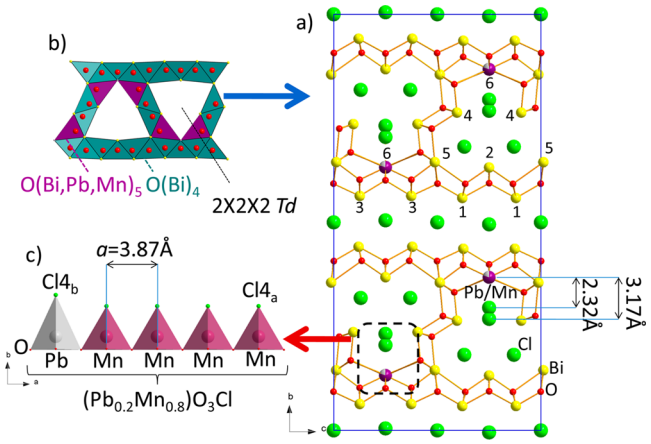

Figure 5. (a) Crystal structure of $Bi_9(Pb_{0.2}Mn_{0.8})O_{12}Cl_5$. (b) The size of the channel: the channel walls are formed by oxocentered OBi_4 tetrahedra (dark green), while the connection of $O(Bi,Pb,Mn)_5$ square-pyramid is highlighted in purple. (c) arrangement of corner-sharing $(Pb_{0.2}Mn_{0.8})O_3Cl$ tetragonal pyramid along the *a*-axis.

Table 6. Bond Lengths (Å) of $Bi_9(Pb_{0.2}Mn_{0.8})O_{12}Cl_5$

atom1	atom2	*d*	atom1	atom2	*d*
Bi1	1×O7	2.176(32)		1×O3	2.280(30)
	2×O4	2.225(15)		2×Cl4b	3.1192(42)
	1×O1	2.330(16)		2×Cl4a	3.2679(59)
	2×Cl1	3.2877(11)		2×Cl3	3.2930(79)
	2×Cl2	3.4586(75)	Bi5	1×O6	2.227(31)
Bi2	2×O4	2.201(31)		2×O5	2.347(17)
	2×O1	2.278(17)		2×O7	2.545(21)
	4×Cl3	3.1300(83)		1×O3	2.566(26)
Bi3	1×O7	2.207(32)		2×Cl3	3.1886(86)
	1×O2	2.292(17)	Mn/Pb6	2×O2	2.173(15)
	2×O6	2.298(16)		2×O6	2.184(32)
	2×Cl2	3.3229(72)		1×Cl4a	2.317(21)
	2×Cl1	3.4248(12)		1×Cl4b	3.167(96)
Bi4	1×O5	2.171(26)		4×O5	3.472(26)
	2×O3	2.239(16)			

from those in sodium chloride, 2.81 Å bond.[30] Admittedly for Bi/Na(5), Bi/Na(7), and Bi/Na(8) mixed sites are found to be compatible for both cationic types by Bond Valence Sums (BVS) calculations as listed in the Table 3. These results support the above Bi/Na disordered model.

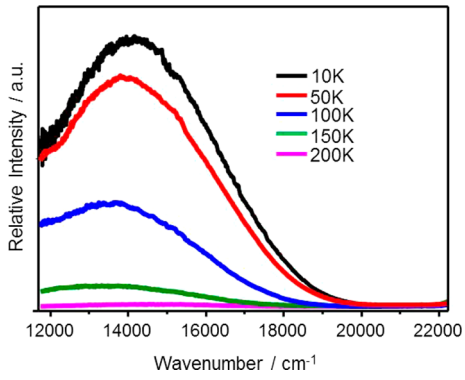

Figure 7. Temperature dependence of $Bi_6NaO_{7,5}Cl_4$ emission (excitation at 410 nm).

We already announced in Table 1 the successful preparation of the corresponding powder using the stoichiometric ratio between all elements. The pattern is shown on Figure 3, although it suffers from severe preferred orientation, probably because of the layered texture.

$Bi_{17}PbO_{22}Cl_9$ (II). The crystal structure of compound (II) was solved in the *C*2/*m* space group (lattice parameters a = 38.9122(18) Å, b = 3.8850(2) Å, c = 11.6784(6) Å, β = 95.729(3)°) and refined similarly as for compound (I). The (*hk*0) precession image calculated from the full data set shows a broadening of the diffraction spots with increasing diffraction angle, suggesting a twinning compatible with a 180° around c (Supporting Information, Figure S3). The consideration of the twinning matrix confirms the reality of this crystal defect improving the R values by more than 3%, leading to a 73%/27% ratio between the main and secondary domains. The structure solution was achieved with fully occupied anionic positions (oxygen and chlorine atoms). In absence of mixed Pb/Bi sites, the final formula is non-neutral, that is, $[Bi_{18}O_{22}Cl_9]^{+1}$. Finally, accordingly to the EDX analysis with evidence of a shoulder on the M_α emission peak, the incorporation of Pb^{2+} is probable as both elements were present in the parent mixture, yielding the neutral formula $Bi_{17}PbO_{22}Cl_9$. Previously, we checked by refining the occupancies of all cationic positions that there was no significant deviation from full occupancies which refutes the presence of Bi^{3+} vacancies in the framework. We have recently shown in the $[Pb_nBi_{10-n}O_{13}][Bi_2O_2]_nCl_{4+n}$ series[20] that the

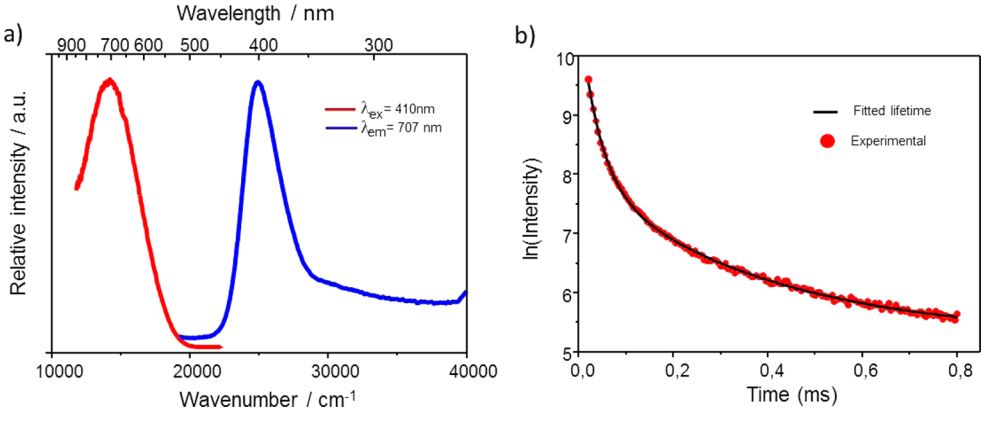

Figure 6. (a) Emission (red) and excitation (blue) spectra of $Bi_6NaO_{7,5}Cl_4$ at 10 K. (b) Lifetime of $Bi_6NaO_{7,5}Cl_4$ measured at 10 K and fitted with a double exponential curve (Adj. R^2 = 0,9986), yielding two different lifetimes of 385 and 40 μs.

dx.doi.org/10.1021/ic402578m | *Inorg. Chem.* 2014, 53, 528−536

localization of Pb/Bi mixed positions in the context of a Birich matrix may be complex, and the distribution of the Pb content over all Bi positions may be possible. However the proposition of an ordered model is relevant in this case since thermal parameters for Bi(7), Bi(8), and Bi(9) are abnormally high (U_{eq} ~ 0.04 Å^2), which reflects a certain degree of disorder possibly because of mixed Bi/Pb positions. Note that these three cationic positions are involved in the OBi_5 square pyramid around O(11), similarly to disordered O(9)Bi_5 for compound (I). Contrary to the compound (I) case, an accurate analysis of the Fourier-maps around O(11) did not reveal pronounced satellite positions but a broad local electron density. By analogy to the split of Bi(6) in compound (I) (see Figure 1c,d), we decided to assign a 25% Pb/75% Bi mixed occupancy to Bi/Pb(7) and Bi/Pb(8) sites. We note that the BVS calculations in the Bi^{3+}/Pb^{2+} hypotheses lead to 2.38/2.36 and 2.27/2.25, respectively, for M(7) and M(8) sites, which seems well adapted for lead incorporation, see Table 3. In this table, note that BVS parameters for Pb were calculated using recent Krivovichev's parameters [31] while for other atoms it was taken from ref 32. The final refined model yields R = 0.0568, wR = 0.0722. Pertinent distances are listed in the Table 5. The crystal structure of (II) is shown on the Figure 4a, and evidences a topology similar to the one of compound (I) but with 2 × 2 × 2 O(Bi,Pb)$_4$-wide triangular channels, Figure 4b. Once again, the rows shaping the triangles are formed of OBi_4 tetrahedra (2.19 Å < Bi-O < 2.45 Å), joined at O(11). The triangular junctions are achieved by O(9)$(Bi,Pb)_5$, leading to three types of bond distances O(11)-Bi(9) = 2.21Å, O(11)-Bi/Pb(7) = 2.70 Å, O(11)-Bi/Pb(8) = 2.71 Å, see Figure 4c−d and Table 5. The channels are parallel to the b- axis and filled by Cl^- ions. The [010] TEM image (Figure 2.II) allows a direct observation of the triangular tunnel sections. No periodicity defect was observed in the selected zone.

The strict segregation of the Cl^- into subunits leads to the general formula $[Bi_{17}PbO_{22}][Cl_6]_{channel}[Cl_3]_{layer}$. If one focuses on the coordination of the cations, a similar VIII-coordination with a tetragonal antiprism is found around Bi(1)-Bi(6), to be compared to the IX-coordination of Bi/Pb(7), Bi/Pb(8), and Bi(9) (two Cl and seven O atoms).

For Bi(1) to Bi(6) atoms, the oxygen coordination is BiO_4 coordination with an average Bi-O distance of 2.27 Å, similar to Bi-O distances in $PbBi_4O_6Cl_2$ [20] and $Bi_{24}O_{31}Cl_{10}$.[27,33] The corresponding powdered phase was prepared in presence of minor secondary phases (i.e., $Bi_{17}Pb_{1-x}O_{22}Cl_9$, $Pb_3O_2Cl_2$ or $Pb(ClO_2)_2$) as given in the Table 1.

$Bi_9(Pb_{0.2}Mn_{0.8})O_{12}Cl_5$ (III). The crystal structure of compound (III) was solved in the space group *Cmcm* (a = 3.8695(2) Å, b = 31.7369(15) Å, c = 15.7602(7) Å). The main part of the structure is fully ordered, but the electron density about position Pb/Mn(6) suggests a mixed position with ratio 0.18/0.82 as refined. It was fixed to 0.2/0.8 for charge balance according to the formula $Bi^{III}_9(Pb^{II}_{0.2}Mn^{II}_{0.8})O_{12}Cl_5$. Concomitantly, in the neighborhood of this site inside the channels, a significant splitting of the next Cl(4) position into $Cl(4)_a$ and $Cl(4)_b$ with suitable occupancies was observed on Fourier-difference maps. This split is consistent with the presence of two different metals Pb/Mn(6) (in terms of radii 1.19 Å vs 0.75 Å) leading to 80% Mn-$Cl(4)_a$ (=2.32 Å), 20% Pb-$Cl(4)_b$ (=3.16 Å). The BVS shown in Table 3 validate the predominant Mn^{2+} character of this mixed site, while the complementary Pb (20%) seems over bonded. It is clear that the local shift of 20% of the oxygen neighbors would not be revealed by XRD. It is noteworthy that the choice for Pb in this site rather than Bi is justified by the original coordination of the Pb/Mn(6) site (see Figure 5a): 4O + 1Cl, rather than the typical 4O + 4Cl antiprism found around most Bi^{3+} for compounds (I), (II), and (III), and by the microprobe analysis, Figure 5c. There is no clue for any ordering between the PbO_4Cl and MnO_4Cl polyhedra from XRD data.

Finally, the refinement of the anisotropic thermal parameters for all Bi/Pb/Cl atoms, the residual factors converged to $R1$ = 0.047 and wR = 0.067 for 72 refined parameters and 1189 used reflections. The refined atomic positions and anisotropic displacement parameters are given in Supporting Information, Tables S6 and S7, respectively. The pertinent distances are listed in the Table 6. The compound corresponds to the formula $[Bi_9(Pb_{0.2}Mn_{0.8})O_{12}]\ Cl_3]_{channel}[Cl_2]_{layer}$.

Once more, it is formed of a single layered fluorite like $[(Bi,Pb,Mn)_2O_2]^{2+}$ layers interconnected by transverse ribbons of OBi_4 tetrahedra into 2 × 2 × 2 triangular channels, Figure 5b. These tunnels are observed well on the [100] TEM image (Figure 2.III). In this compound also, the connection between the channel walls is achieved by penta-coordinated O(5) atoms ($OBi_3(Pb,Mn)_2$) as shown in magenta in the Figure 5b, but their disposition in edge-sharing pairs changes the topology of the channels. Note that the V coordination of O(5) engages very long O(5)-(Pb/Mn(6)) bonds of 3.47 Å. The channels are filled by Cl^- ions. The bismuth atoms are VIII coordinated by four Cl and four O atoms, the Bi−O distances range from 2.20 to 2.30Å, leading to correct BVS calculations, see Table 3.

Luminescence of $Bi_6NaO_{7,5}Cl_4$. Since the 1930s, many investigations about the optical properties of ns^2 ions (Bi^{3+}, Pb^{2+}, Tl^+, Sb^{3+})[34,35] are described thoroughly, because these cations exhibit in general an extremely bright emission thanks to the $s^2 \leftrightarrow sp$ allowed electronic transition. Therefore, some of these ns^2 based compounds are used for applications, for example, BGO ($Bi_4Ge_3O_{12}$) is well suited in scintillators.[36] Other compounds are very promising for lightening purposes to substitute the generally used lanthanide materials for resource saving reasons. s^2 ions exhibit a singlet $^1S_0$ ground state while the excited states with sp configuration give rise to triplet ($^3P_0$, $^3P_1$, and $^3P_2$, in order of increasing energy) and singlet ($^1P_1$) states. Although all transitions between the ground and excited states are parity allowed, the lowest energy transition $^1S_0 \leftrightarrow {}^3P_0$ is strongly forbidden because of spin and angular momentum selection rules. The transitions from the ground state to $^3P_1$ (A-band, spin forbidden) and $^3P_2$ (B-band, spin and angular momentum forbidden) are allowed because of spin−orbit coupling between $^3P_1$ and $^1P_1$ states and coupling to the asymmetrical photon mode, respectively. Transition from ground state $^1S_0$ to the singlet $^1P_1$ is an allowed electronic dipole (C-band).[37] In some cases the D-band is also observed, which corresponds to the charge transfer state of the ns^2 ion and the ligand. The intensities of the emission bands are not only influenced by the selection rules, but mainly by the population of the excited states, so that also forbidden transitions can be observed with remarkably efficiency. In this paper we present the luminescence properties of $Bi_6NaO_{7,5}Cl_4$, the only of the three new compounds described here which was prepared as single phase.

$Bi_6NaO_{7,5}Cl_4$ shows a bright red emission at low temperatures which is scarcely observed for Bi^{3+} ions. The emission and excitation spectra measured at 10 K are presented in Figure 6a. The emission band consists of a broad band starting at about 19000 cm^{-1} with a maximum at 14140 cm^{-1} (707 nm)

dx.doi.org/10.1021/ic402578m | Inorg. Chem. 2014, 53, 528−536

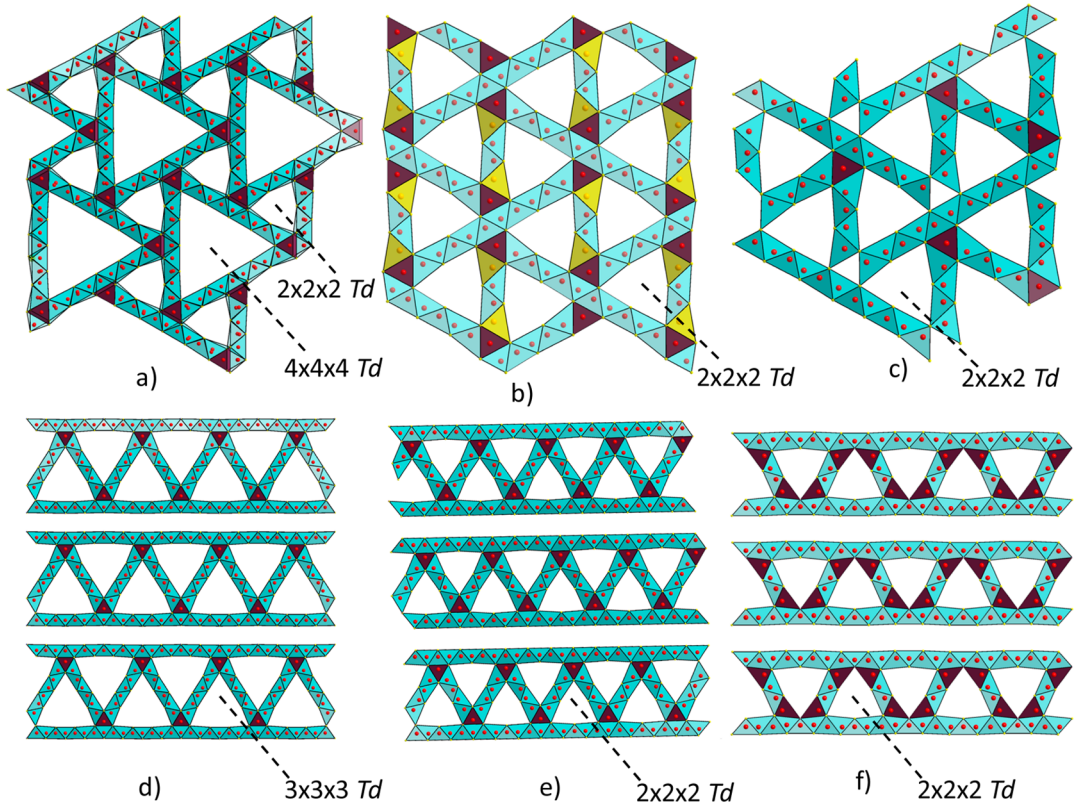

Figure 8. Comparison of the Porous 3D networks of $O(Bi,M)_4$tetrahedra in light blue (the tunnel junctions by $O(Bi,M)_5$ square-pyramids is highlighted in purple): (a) $(Ag_{4.78}\ Cl_{1.5})(Bi_{48}\ O_{58.64}\ Cl_{30})$, (b) $[Bi_6O_6F]OCl_3$ ($F(Bi,M)_4$ tetrahedra is remarked in yellow), (c) $Bi_{12}O_{15}Cl_6$, (d) $Bi_6NaO_{7.5}Cl_4$, (e) $Bi_{17}PbO_{22}Cl_9$, (f) $Bi_9(Pb_{0.2}Mn_{0.8})O_{12}Cl_5$.

and can be assigned to both $^3P_0 \rightarrow {}^1S_0$ and $^3P_1 \rightarrow {}^1S_0$ transitions. This is proven by lifetime measurements at 10 K. The curve was fitted using a double exponential decay function ($I(t) = I_0 + A_1 \exp(-t/\tau_1) + A_2 \exp(-t/\tau_2)$, where A and τ are pre-exponential terms and lifetimes for the two individual decays). Two strongly different lifetimes with comparable weights were found for the emission process A1 = 2.78(5), τ_1 = 41.3(2) μs and A2 = 2.71(2), τ_2 = 380(10) μs leading to a reliable matching (see Figure 6b). The shorter one can be attributed to $^3P_1 \rightarrow {}^1S_0$, while the longer one to $^3P_0 \rightarrow {}^1S_0$ according to the selection rules.[38] The unusual low energy position of the emission band is expected for Cl^- ligands because of the electronic cloud expansion occurring from partial orbital overlapping with voluminous Cl^- ions (nephelauxetic effect) compared to full-oxygen coordination. By comparison to luminescence properties of other oxohalides, for example, Sillèn phases $SrBiO_2Cl$, $BaBiO_2Cl$ and $BaBiO_2Br$ with emission maxima at 430 nm, 490 nm, and 500 nm, respectively,[23] with much longer Bi-Cl bond lengths (~ 3.6 Å in $BaBiO_2Cl$), the emission position at ~700 nm in $Bi_6NaO_{7.5}Cl_4$ is also well explained by greater covalent bonds (nephelauxetic effect). We already observed a similar behavior than in the present work for $PbBi_4O_6Cl_2$ and $BaBi_4O_6Cl_2$ with comparable Bi coordinations.[20]

The maximum of the excitation band culminates at 24390 cm^{-1} which corresponds to the A-band because of its large intensity. The large Stokes shift of 10250 cm^{-1} is usual for Bi^{3+} because of off-centering between the fundamental (nominally $6s^2\ 6p^0$) and excited states (nominally $6s^1\ 6p^1$).[38] Despite the important number of Bi sites, one notices single but broad emission and excitation bands in the absence of any shoulder probably due to similar Cl/O coordination (predominant BiO_4Cl_4 antiprism). Although the $^3P_0$ and $^3P_1$ states could be very close in energy, the broadness of the emission band (FWHM > 5000 cm^{-1}), however, concomitantly with the eight individual Bi(1−8) contributions do not allow. As a proper explanation of this observation, energy transfer $^3P_1 \rightarrow {}^3P_0$ and also between the crystallographically different Bi^{3+} ions can be assumed, which would confine the emission band to the low lying states. However, this behavior should be also condensed in a very short lifetime component, which we could not investigate because of limited equipment.

Figure 7 shows the temperature dependence of the emission intensity for $Bi_6NaO_{7.5}Cl_4$. Above 200 K the luminescence is totally quenched. The emission intensity decreases with increasing temperature, which is accompanied by a strong red shift of the emission maxima (13642 cm^{-1} at 100 K). This common behavior is due to lattice contraction and shortening of the Bi-O/Bi-Cl bond distances,[35] but it is still a drawback for applications as lamp phosphors.

(3). CONCLUDING REMARKS

While the literature is paved with examples of layered Bi based oxo-halides, the existence of 1D channels is scarce, even if not novel. To the best of our knowledge, oxocentered ribbons condensed to create triangular channels have already been observed in three compounds, $[Bi_{48}O_{58.64}][Ag_{4.78}Cl_{31.5}]_{channel}$,[39] $[Bi_6O_7F][Cl_3]_{channel}$,[40] and $[Bi_{12}O_{15}][Cl_6]_{channel}$[22] (Figure 8a,b,c), and are listed as typical examples of porous 3D-frameworks formed of oxocentered tetrahedra in the related review.[18] They respectively exhibit 2 × 2 × 2 T_d and 4 × 4 × 4 T_d triangular pores filled by Ag^+ and Cl^- ions in the former and

dx.doi.org/10.1021/ic402578m | Inorg. Chem. 2014, 53, 528−536

only 2 × 2 × 2 T_d pores in the two later compounds. Similarly to the three title compounds shown in the Figures 8d,e,f, the triangular junctions are ensured by the OBi_5 square pyramid in $[Bi_{48}O_{58.64}][Ag_{4.78}Cl_{31.5}]_{channel}$ [39] and $[Bi_6O_6F]OCl_3$,[40] while empty $\square Bi_5$ also participate in $[Bi_{12}O_{15}][Cl_6]_{channel}$.[22]

Note in the second compound that FBi_4 tetrahedra (shown in yellow in Figure 7b) also participate to the channel edges. However, in compound (III), the 2 × 2 × 2 T_d channel sections are modified because of two OBi_5 sharing edges together. Also it is worth noting that on the basis of the litterature, the 3 × 3 × 3 T_d channels of compound (I) are unique.

In addition, the key novelty of these compounds is based to the association of layers and pores never observed to date in related materials of similar phase diagrams. Among the broad interest due to the degree of architecture found here, this paper illustrates well the structural complexity and versatility offered in the Bi-O-Cl phase diagram. Particularly the diversity of frameworks built on the association of $(OBi)_4$ tetrahedra opens the possibility to rationally control the size and/or geometry of pores as well as their association in predicted crystal structures. Finally the redshift observed for luminescence, compared to bismuth oxides, is rather interesting, and chlorides appear as promising ligands to tune optical properties.

■ ASSOCIATED CONTENT

Supporting Information

Crystallographic tables, EDX spectra, and complementary bismuth oxochlorides crystal structure representations. This material is available free of charge via the Internet at http://pubs.acs.org.

■ AUTHOR INFORMATION

Corresponding Author

*E-mail: olivier.mentre@ensc-lille.fr.

Notes

The authors declare no competing financial interest.

■ ACKNOWLEDGMENTS

The Fonds Européen de Développement Régional (FEDER), CNRS, Région Nord Pas-de-Calais, and Ministère de l'Education Nationale de l'Enseignement Supérieur et de la Recherche are acknowledged for funding the X-ray diffractometers. Laurence Burylo and Nora Djellal are thanked for their precious technical help. This work was carried out under the framework of the Multi-InMaDe project supported by the ANR (Grant ANR 2011-JS-08 003 01).

■ REFERENCES

(1) Blasse, G.; Sytsma, J.; Brixner, L. H. *Chem. Phys. Lett.* **1989**, *155*, 64−68.
(2) Wu, S.; Wang, C.; Cui, Y.; Wang, T.; Huang, B.; Zhang, X.; Qin, X.; Brault, P. *Mater. Lett.* **2010**, *64*, 115−118.
(3) Burch, R.; Chalker, S.; Loader, P.; Thomas, J. M.; Ueda, W. *Appl. Catal., A* **1992**, *82*, 77−90.
(4) Liu, S.; Miiller, W.; Liu, Y.; Avdeev, M.; Ling, C. D. *Chem. Mater.* **2012**, *24*, 3932−3942.
(5) Sillén, L. G. *Z. Anorg. Allg. Chem.* **1939**, *242*, 41−46.
(6) Sillén, L. G. *Naturwissenschaften* **1942**, *30*, 318−324.
(7) Gilberg, M. *Ark. Kemi Mineral. Geol.* **1960**, *B2*, 565.
(8) Kirik, S. D.; Yakovleva, E. G.; Shimanskii, A. F.; Kovalev, Y. G. *Acta Crystallogr.* **2001**, *C57*, 1367−1368.
(9) Fray, S. M.; Milne, C. J.; Lightfoot, P. *J. Solid State Chem.* **1997**, *128*, 115−120.
(10) Keramidas, K. G.; Voutsas, G. P.; Rentzeperis, P. I. *Z. Kristallogr.* **1993**, *205*, 35−40.
(11) Lopatin, S. Ž. *Neorg. Khim.* **1987**, *32*, 1694−1697.
(12) Charkin, D. O.; Berdonosov, P. S.; Dolgikh, V. A.; Lightfoot, P. *J. Solid State Chem.* **1997**, *128*, 316−321.
(13) Charkin, D. O.; Kazakov, S. M.; Lebedev, D. N. *Russ. J. Inorg. Chem.* **2010**, *55*, 1248−1256.
(14) Charkin, D. O. *Russ. J. Inorg. Chem.* **2008**, *53*, 1977−1996.
(15) Sillen, L. G. *Z. Anorg. Allg. Chem.* **1941**, *246*, 115−126.
(16) Zhu, W.-J.; Huang, Y. Z.; Liang, J.-K.; Zhao, Z.-X. *Mater. Res. Bull.* **1992**, *27*, 885−890.
(17) Sillen, L. G.; Gjoerling-Husberg, A. S. *Z. Anorg. Allg. Chem.* **1941**, *248*, 121−134.
(18) Krivovichev, S. V.; Mentré, O.; Siidra, O. I.; Colmont, M.; Filatov, S. K. *Chem. Rev.* **2013**, *113*, 6459−6535.
(19) Krivovichev, S. V.; Filatov, S. K. *Crystal chemistry of minerals and inorganic compounds with complexes of anion-centered tetrahedra*; St. Petersburg University Press: St. Petersburg, Russia, 2001.
(20) Aliev, A.; Olchowka, J.; Colmont, M.; Capoen, E.; Wickleder, C.; Mentré, O. *Inorg. Chem.* **2013**, *52*, 8427−8435.
(21) Arppe, A. E. *Ann. Phys. Chem.* **1845**, *140*, 237−251.
(22) Hopfgarten, F. *Acta Crystallogr.* **1976**, *B32*, 2570.
(23) Porter-Chapman, Y.; Bourret-Courchesne, E.; Derenzo, S. E. *J. Lumin.* **2008**, *128*, 87.
(24) *SAINT, Area-Detector Integration Software*; Siemens Industrial Automation, Inc.: Madison, WI, 1996.
(25) *SADABS, Area-Detector Absorption Correction*; Siemens Industrial Automation, Inc.: Madison, WI, 1995.
(26) Stadelmann, P. *JEMS*, ems java version; CIME-EPFL: Lausanne, Switzerland, 1999−2003.
(27) Sillen, L. G.; Edstrand, M. *Z. Kristallogr.* **1942**, *104*, 178−196.
(28) Sheldrick, G. M. *SHELXS-97, Programs for X-ray Crystal Structure Solution*; University of Göttingen: Göttingen, Germany, 1997.
(29) Darriet, J.; Launay, J. C.; Zuniga, F. J. *J. Solid State Chem.* **2005**, *178*, 1753.
(30) Abrahams, S. C.; Bernstein, J. L. *Acta Crystallogr.* **1965**, *18*, 926−932.
(31) Krivovichev, S. V. *Z. Kristallogr.* **2012**, *227*, 575−579.
(32) Brese, N. E.; O'Keeffe, M. *Acta Crystallogr.* **1991**, *B47*, 192−197.
(33) Eggenweiler, U.; Keller, E.; Krämer, V. *Acta Crystallogr.* **2000**, *B56*, 431−437.
(34) Timmermans, C. W. M.; Blasse, G. *J. Solid State Chem.* **1984**, *52*, 222.
(35) Blasse, G. *J. Lumin.* **1997**, *72*−*74*, 129.
(36) Folkerts, H. F.; Zuidema, J.; Blasse, G. *Chem. Phys. Lett.* **1996**, *249*, 59.
(37) Setlur, A. A.; Srivastava, A. M. *Opt. Mater.* **2006**, *29*, 410.
(38) Boulon, G.; Moine, B.; Bourcet, J. C. *J. Lumin.* **1979**, *18/19*, 924.
(39) Aurivillius, B. *Acta Chem. Scand.* **1990**, *44*, 111.
(40) Hopfgarten, F. *Acta Crystallogr.* **1975**, *B31*, 1087.